

# Structural and functional implications of the alternative complement pathway C3 convertase stabilized by a staphylococcal inhibitor

Suzan H M Rooijakkers<sup>1,5</sup>, Jin Wu<sup>2,5</sup>, Maartje Ruyken<sup>1</sup>, Robert van Domselaar<sup>1</sup>, Karel L Plancken<sup>3</sup>, Apostolia Tzekou<sup>4</sup>, Daniel Ricklin<sup>4</sup>, John D Lambris<sup>4</sup>, Bert J C Janssen<sup>2</sup>, Jos A G van Strijp<sup>1</sup> & Piet Gros<sup>2</sup>

Activation of the complement system generates potent chemoattractants and leads to the opsonization of cells for immune clearance. Short-lived protease complexes cleave complement component C3 into anaphylatoxin C3a and opsonin C3b. Here we report the crystal structure of the C3 convertase formed by C3b and the protease fragment Bb, which was stabilized by the bacterial immune-evasion protein SCIN. The data suggest that the proteolytic specificity and activity depend on the formation of dimers of C3 with C3b of the convertase. SCIN blocked the formation of a productive enzyme-substrate complex. Irreversible dissociation of the complex of C3b and Bb is crucial to complement regulation and was determined by slow binding kinetics of the Mg<sup>2+</sup>-adhesion site in Bb. Understanding the mechanistic basis of the central complement-activation step and microbial immune evasion strategies targeting this step will aid in the development of complement therapeutics.

Complement is an ancient defense mechanism that evolved into a large protein-interaction network in mammals that initiates and serves innate immune functions and links innate immunity with adaptive immunity<sup>1</sup>. Activation of complement is critical for protection against microbial infection; however, over-activation of complement causes host tissue damage<sup>2</sup>. The complement system is initiated either by specific recognition of target cells in the classical and lectin pathways or spontaneously because of inherent instability of complement component C3 in the alternative pathway<sup>3</sup>. These pathways converge in the formation of C3 convertases, which cleave C3 into the small anaphylatoxin C3a and the large, reactive C3b that may covalently couple to target surfaces<sup>4,5</sup>. In the amplification loop of the alternative pathway, proenzyme factor B (FB) binds to surface-bound C3b and is cleaved by factor D (FD), which results in an active convertase complex that consists of C3b and the noncovalently bound protease fragment Bb (C3bBb). These convertases amplify C3b production near the target surface, which results in rapid opsonization of the target cell with C3b, which can then elicit B cell stimulation, phagocytosis and cell lysis<sup>1</sup>. Similarly, C3 convertases are formed in the classical and lectin pathways by C4 and C2, which are homologs of C3 and FB, respectively<sup>6</sup>. Both C3 convertases (C3bBb and C4b2a) are active only toward their natural substrate C3, with limited activity toward the homolog C5 (ref. 7). In the terminal complement pathway, the substrate specificity is switched from C3 to C5 after association of one or more C3b molecules with the C3bBb or C4b2a complex<sup>8,9</sup>.

Regulation of activity is achieved by convertase assembly and disassembly, which is mediated by complement regulators<sup>10</sup>. For this regulation, it is essential that enzymatic activity toward C3 is expressed only by the assembled active convertases (C3bBb and C4b2a) and not by the proenzymes (FB and C2), proenzyme complexes (C3bB and C4bC2) or dissociated fragments (Bb and C2a). In addition, the convertases are meta-stable and dissociate irreversibly (with an inherent half-life of 60–90 s at 37 °C)<sup>11</sup>; therefore, the protease fragments Bb or C2a do not reassociate with C3b or C4b, respectively. In this way, the protease activity of the short-lived C3 convertase complexes determines opsonization of pathogens and altered host cells, which is a pivotal step in raising complement-mediated immune responses.

To resist the host immune response, pathogenic bacteria and viruses have evolved many well-defined strategies to evade the immune system. Because the complement system is a key element in antibacterial defense, many of these evasion molecules are directed against complement components. Blocking the central activation step of C3 to C3b is a principal bacterial complement-evasion strategy: streptococci secrete molecules that degrade the C3 molecule, whereas many pathogens indirectly block C3 convertases by attracting host convertase regulators to their surfaces<sup>12</sup>. Staphylococcal complement inhibitor (SCIN) from *Staphylococcus aureus* has been described as a bacterial protein that directly targets C3 convertases<sup>13</sup>. SCIN is found in 90% of *S. aureus* strains and specifically binds active convertases (C3bBb and C4b2a) on bacterial surfaces and prevents opsonization of

<sup>1</sup>Medical Microbiology, University Medical Center Utrecht, Utrecht, The Netherlands. <sup>2</sup>Crystal and Structural Chemistry, Bijvoet Center for Biomolecular Research, Department of Chemistry, Faculty of Science, and <sup>3</sup>Van 't Hoff Laboratory for Physical and Colloid Chemistry, Utrecht University, Utrecht, The Netherlands. <sup>4</sup>Department of Pathology & Laboratory Medicine, University of Pennsylvania, Philadelphia, Pennsylvania, USA. <sup>5</sup>These authors contributed equally to this work. Correspondence should be addressed to P.G. (p.gros@uu.nl).

Received 11 March; accepted 15 May; published online 7 June 2009; doi:10.1038/ni.1756

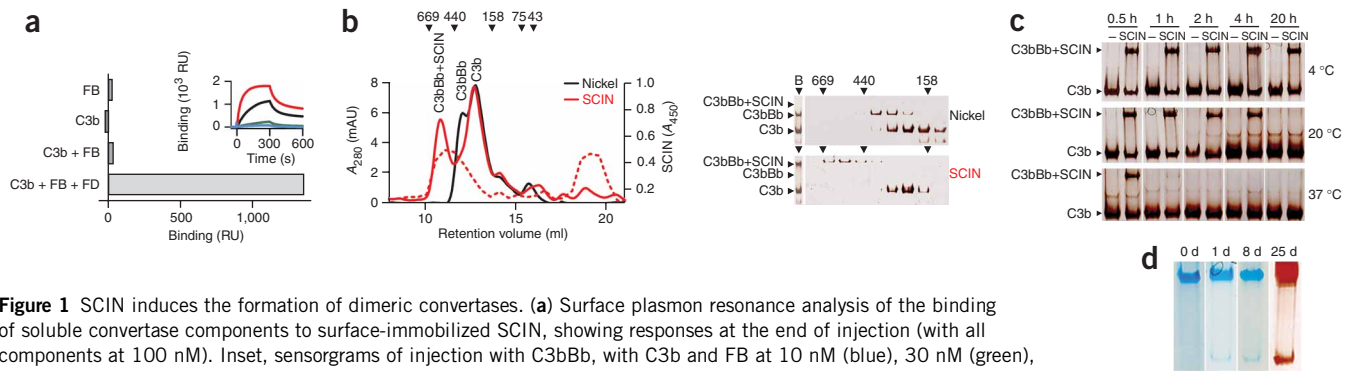


**Figure 1** SCIN induces the formation of dimeric convertases. **(a)** Surface plasmon resonance analysis of the binding of soluble convertase components to surface-immobilized SCIN, showing responses at the end of injection (with all components at 100 nM). Inset, sensorgrams of injection with C3bBb, with C3b and FB at 10 nM (blue), 30 nM (green), 100 nM (black) or 300 nM (red), and FD at 100 nM. RU, resonance units. **(b)** Gel-filtration analysis (left) and native gel electrophoresis (right) of SCIN-inhibited convertases. Left, absorbance at 280 nm ( $A_{280}$ ) of active convertases stabilized by  $\text{Ni}^{2+}$  (Nickel) and SCIN-inhibited convertases (SCIN). The 178-kDa peak corresponds to free C3b. Dashed red line, elution positions of SCIN determined by enzyme-linked immunosorbent assay (right axis; absorbance at 450 nm). mAU, milli-absorbance units. Right, electrophoresis of active convertase (Nickel) and SCIN-inhibited convertase (SCIN) before gel filtration (B) and of fractions eluted from the gel filtration column. **(c)** Analysis of the stability of C3b (500 nM), FB (500 nM), FD (250 nM) and SCIN (1  $\mu\text{M}$ ) incubated for various times (above) at 4 °C, 20 °C or 37 °C and separated by native gel electrophoresis at 4 °C. No complexes are present in the absence of SCIN (–). **(d)** Native gel electrophoresis of purified SCIN-convertase complexes after 0–8 d (left; Coomassie staining) and 25 d (far right; silver staining). Data are representative of three (**a–c**) or two (**d**) independent experiments.

bacteria and subsequent phagocytosis<sup>13</sup>. A notable characteristic of SCIN is that it stabilizes convertases on bacterial surfaces, and mutational analyses indicate that this is essential for its inhibitory function<sup>14</sup>.

Structural studies of the C3 convertases are challenging because these complexes dissociate irreversibly and have short half-lives. Here we used SCIN to stabilize the C3 convertase of the alternative pathway (C3bBb) and to crystallize C3bBb in complex with SCIN. The structure gave insight into the inhibitory mode of SCIN and provided a structural basis for the enzymatic activity, substrate specificity and irreversible dissociation of the C3 convertases that are central to immune defense.

## RESULTS

### SCIN induces the formation of stable convertase dimers

First we studied whether SCIN, an inhibitor of surface-bound convertases, also binds and stabilizes soluble convertases. Using surface plasmon resonance, we found that surface-immobilized SCIN specifically bound C3bBb (generated in solution by mixture of C3b, FB and FD) and not FB, C3b or proconvertase C3bB (Fig. 1a). Incubation of histidine-tagged SCIN with C3b, FB and FD in solution resulted in simultaneous association of C3b and Bb with SCIN, whereas no complexes were formed in the absence of FD or FB (Supplementary Fig. 1 online). SCIN inhibited convertases in solution, as C3bBb did not cleave C3 in the presence of SCIN (Supplementary Fig. 2 online). Gel-permeation chromatography of the complexes generated in the presence of SCIN showed that SCIN induced the formation of large complexes of ~500 kilodaltons (kDa), twice the size of an active convertase complex (~240 kDa; Fig. 1b). Immunoblot analysis and enzyme-linked immunosorbent assay showed that these complexes indeed contained C3b, Bb and SCIN (Fig. 1b and Supplementary Fig. 3 online). We also detected the SCIN-induced formation of large convertase complexes by native gel electrophoresis, and we used this method to analyze the stability of complexes (Fig. 1b,c). At 20 °C, SCIN-stabilized complexes had a half-life of up to 4 h, whereas at 4 °C, we noted an improvement in stability, with a half-life exceeding 20 h (Fig. 1c). For crystallization purposes, we optimized the stability of the complex in small-scale experiments comparing a variety of purification methods, which allowed us to generate highly stable complexes in the milligram range. We used SCIN with a histidine-tag at the amino

(N) terminus to generate complexes in fluid phase that we then purified from reactants (such as FD, Ba and excess C3b and FB) with magnetic  $\text{Co}^{2+}$  beads. We used ultrafiltration to remove SCIN not in complex and to further concentrate the samples. For crystallization, we generated 10  $\mu\text{M}$  complexes (approximately 5 mg/ml) that were stable over 25 d at 4 °C (Fig. 1d). Analytical ultracentrifugation of the purified material showed a major component of 15.2 S and a minor component of ~18 S, which probably corresponded to the SCIN-stabilized dimeric complex of ~500 kDa and a putative dimer of dimers, respectively (Supplementary Fig. 4 online). Thus, SCIN bound and blocked active convertases in solution and induced the formation of dimers of C3bBb. The stabilizing ability of SCIN allowed us to generate highly pure and stable convertase complexes.

### Crystal structure of the SCIN-inhibited convertase

We used freshly prepared and purified SCIN-stabilized complexes to set up crystallization experiments at 4 °C. Crystals appeared within 1–2 d; electrophoresis showed that the crystals consisted of C3b, Bb and SCIN (Supplementary Fig. 5 online). We optimized the crystallization conditions, which resulted in a crystal that diffracted to a resolution of 3.9 Å (crystallographic statistics, Table 1; electron density quality, Supplementary Fig. 6 online). We solved the structure by molecular replacement with the available structures of the individual proteins present in the complex and refined it with noncrystallographic symmetry and tight geometry restraints. The final model was refined to  $R$  and  $R_{\text{free}}$  factors of 25.3% and 26.8%, respectively.

The asymmetric unit contained two complexes, each consisting of a C3bBb-SCIN dimer of 500 kDa with overall dimensions of  $177 \times 168 \times 155$  Å (Fig. 2a). The dimer was built of a C3b-C3b homodimer that was stabilized by bridging SCIN molecules (Fig. 2; complex interface analysis, Supplementary Table 1 online). Each C3b molecule had a typical arrangement of 12 domains, as found in other structures of C3b<sup>15,16</sup>, which consisted of a core formed by eight macroglobulin (MG) domains and a linker domain, a CUB domain ('complement C1r-C1s, UEGF, BMP1') and thioester-containing domain (TED) inserted between MG7 and MG8, and a carboxy (C)-terminal C345C domain (Fig. 2b). Two Bb molecules were positioned symmetrically on the outer edges of the C3b-C3b dimer. Bb was attached to the C-terminal C345C domain of C3b through the

**Table 1** Data collection and refinement statistics

<b>Data collection</b>	
Space group	$P2_1$
Cell dimensions	
<i>a</i> , <i>b</i> , <i>c</i> (Å)	228.6, 121.5, 280.8
$\alpha$ , $\beta$ , $\gamma$ (°)	90, 91.6, 90
Resolution (Å)	40–3.9 (4.11–3.9)
$R_{\text{merge}}$ (%)	12.8 (69.0)
$I/\sigma I$	10.4 (1.8)
Completeness (%)	97.6 (92.0)
Redundancy	3.5 (3.4)
<b>Refinement</b>	
Resolution (Å)	39.8–3.9
Reflections	137,476
$R_{\text{work}}/R_{\text{free}}$ (%)	25.3/26.8
Atoms	67,989
Protein	67,266
Ligand/ion	723
Water	
B-factors (Å <sup>2</sup> )	
Protein	158
Ligand/ion	208
Water	
r.m.s.d.	
Bond lengths (Å)	0.002
Bond angles (°)	0.519

Values in parentheses are for the shell of highest resolution. 'Ligand/ion' indicates the modeled MIDAS Mg<sup>2+</sup> ion, water and glycan chains.

Von Willebrand factor type A (VWA) domain with the active site in the serine protease (SP) domain oriented outward.

### Inhibition of C3bBb by SCIN

SCIN stabilized the convertase dimer by interacting with C3b and Bb of one convertase (with contact areas of  $\sim 1,400 \text{ \AA}^2$  each to C3b and Bb) and with C3b of the opposing convertase (contact area of 1,800  $\text{ \AA}^2$ ; **Fig. 3a** and **Supplementary Fig. 7** and **Table 1** online). SCIN bound the first C3b at its  $\alpha'$  N-terminal tail and domains MG6 and MG7, whereas the binding site in the second C3b was formed by domains MG7 and MG8. SCIN did not block the catalytic site in Bb. Instead, SCIN mainly bound the VWA domain and the VWA-SP interface of Bb (**Fig. 2b** and **Supplementary Fig. 7**). Studies of a panel of eight different chimeras of SCIN and a nonfunctional homolog have identified two segments of SCIN that are essential for activity on bacterial surfaces<sup>14</sup>. These segments (residues 26–36 and 37–48; exchanged in chimeras Ch $\alpha$ 1C and Ch $\alpha$ 2N, respectively) coincided with most of the contact sites for Bb and C3b of one convertase enzyme (**Fig. 3b**). We retested the same eight mutants and found that residues 26–48 were also critical for blocking C3 conversion by convertases in solution, which confirmed the observed arrangement in the crystal (**Fig. 3c**). Next we addressed the importance of the formation of convertase dimers in the inhibition by SCIN. Two SCIN chimeras with altered C3b dimer-formation contact sites (ChN and ChC3b2) yielded stable but monomeric C3bBb-SCIN complexes (**Fig. 3d**). Moreover, these two chimeras still inhibited convertase activity in solution and stabilized convertases on bacteria (**Fig. 3c**). These data confirmed the existence of a dimer-formation site as observed in the complex but demonstrated that the formation of convertase dimers was not essential for the inhibitory activity of SCIN. We therefore conclude that SCIN probably inhibits monomeric

convertases either by blocking substrate binding or by preventing critical movements required for the formation of active enzyme-substrate complexes.

### Architecture of the C3 convertase

In the SCIN-stabilized complex, we noted a loose arrangement of the C3 convertase C3bBb in which Bb seemed to 'dangle' from the tip of the C3b structure. Bb contacted the C-terminal C345C domain of C3b through its VWA domain. We found no contacts between the SP domain of Bb and C3b. This arrangement of C3bBb in the inhibited complex was consistent with published three-dimensional electron microscopy reconstructions of C3bB and C3bBb at a resolution of 27 Å (ref. 17). Most notably, the C-terminal asparagine residue at position 1641 (Asn1641) of C3b chelated the Mg<sup>2+</sup> bound to the metal ion-dependent adhesion site (MIDAS) formed by three loops ( $\beta$ A- $\alpha$ 1,  $\alpha$ 3- $\alpha$ 4 and  $\beta$ D- $\alpha$ 5) of the VWA domain of Bb<sup>18,19</sup> (**Fig. 4a,b**). This arrangement is in full agreement with mutagenesis data on the critical importance of the MIDAS for convertase activity<sup>20,21</sup>. The three loops of the MIDAS contributed to the C3bBb interface; two of these ( $\beta$ A- $\alpha$ 1 and  $\beta$ D- $\alpha$ 5) have been shown to be critical for convertase stability<sup>22</sup> (**Fig. 4b**). In addition, helix  $\alpha$ 6 of the VWA domain of Bb was near the  $\alpha'$  N-terminal tail of C3b (**Fig. 4b**). Published data support the possible existence of a putative secondary interaction site that may be disrupted by SCIN, as substitution of an alanine residue for the asparagine residue at position 415 (N415A) in VWA helix  $\alpha$ 6 of FB yields convertases that are more prone to dissociation by complement regulators<sup>23</sup>. As for C3b, the interface was formed by loops of residues 1515–1520, 1547–1556 and the C-terminal tail (residues 1634–1641) in the C345C domain (**Fig. 4b**). Variation in the C345C orientation (**Supplementary Fig. 8** online) indicated weak interactions of C345C with the  $\alpha$ 3- $\alpha$ 4 loop of VWA that resulted in buried surface areas that ranged from 600  $\text{ \AA}^2$  to 1,200  $\text{ \AA}^2$  (**Supplementary Table 1**). These variations are in agreement with published data showing a limited effect of substitution in the  $\alpha$ 3- $\alpha$ 4 loop on convertase stability<sup>22</sup> (**Fig. 4b**).

The SCIN-stabilized C3bBb complex allowed us to study the effects of complex formation on the conformations of C3b and the proteolytic fragment Bb. The domain arrangement of C3b in the complex (**Supplementary Fig. 9** online) was similar to that of other C3b structures<sup>15,16</sup>; variations in the C345C and CUB-TED domains are common and indicate inherent flexibility of C3b. The structure of the Bb fragment in the C3 convertase was similar to that of free Bb<sup>24</sup>, which is very different from that of the full-length proenzyme FB<sup>25</sup> (**Fig. 4c** and **Supplementary Fig. 10** online). The MIDAS arrangement in C3bBb suggested a typical high-affinity ligand-binding configuration, similar to the structures of free Bb and C2a<sup>24,26</sup> and activated integrin I $\alpha$  domains<sup>27</sup> (**Supplementary Fig. 10**); however, the low resolution of the diffraction data did not allow detailed interpretation. The nascent N-terminal tail of Bb and the VWA helix  $\alpha$ 7, which are putatively conformationally coupled to the MIDAS, adopted positions as in free C2a<sup>26</sup> (**Fig. 4c**). The published structure of free Bb is in part distorted because the construct lacks the seven N-terminal residues and has an introduced disulfide bridge (Cys428–Cys435) that distorts helix  $\alpha$ 7 (ref. 24; **Fig. 4c**). Nevertheless, the VWA-SP orientations in bound versus free Bb differed by only 10°, which indicates limited overall effects of these distortions at the VWA-SP interface. Moreover, SCIN interacted with Bb at the VWA-SP interface; these interactions did not have an apparent effect on the VWA and SP conformations. In contrast, the VWA-SP orientations in C2a and C3bBb differed by 28°, which is possibly an inherent difference between Bb and C2a (**Supplementary Fig. 10a,b**). Overall,

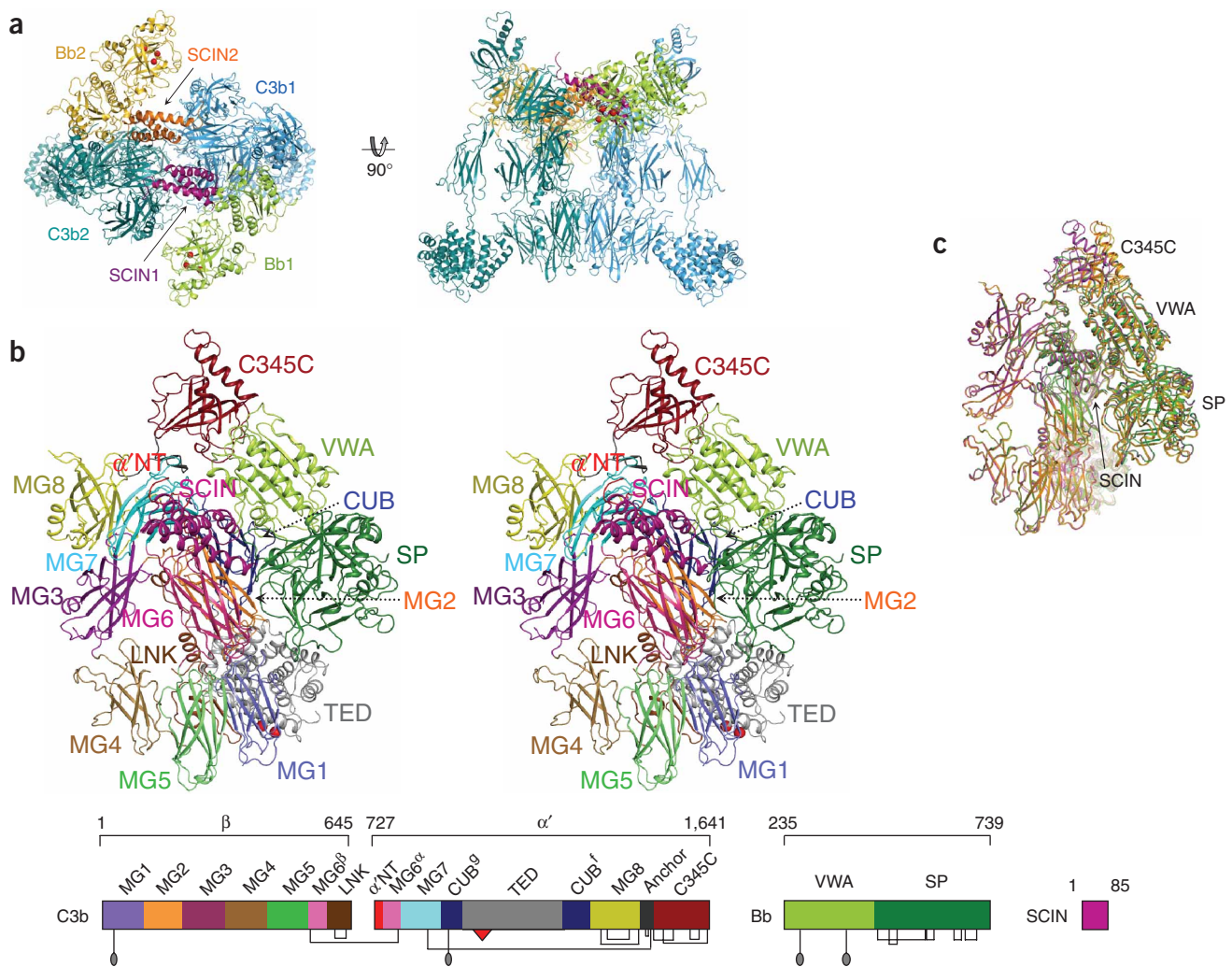


**Figure 2** Crystal structure of the C3 convertase C3bBb inhibited by SCIN. (a) The C3bBb-SCIN dimeric complex, presented as a ribbon diagram with C3b in blue and turquoise, Bb in green and gold and SCIN in purple and orange. (b) 'Stereo' view of the monomeric C3bBb-SCIN extracted from the dimer, with colors indicating protein (SCIN) or protein domain (VWA and SP of Bb, and all 12 domains of C3b, with red spheres indicating thioester); below, domain composition (including disulfide bonds, glycosylation sites and thioester).  $\alpha'$ -NT,  $\alpha'$  N-terminal tail. (c) Overlay of the four C3bBb-SCIN complexes in the asymmetric unit (yellow, orange, green and magenta; additional details, **Supplementary Fig. 8** online).

the conformation of the components C3b and Bb in the convertase complex are similar to those of the isolated C3b and Bb proteins.

### Implications for enzymatic activity and specificity

The active site in the SP domain in C3bBb showed a typical catalytic serine–histidine–aspartic acid triad and oxyanion hole. The oxyanion-hole loop (residues 672–674), however, was distorted because of a peptide 'flip' in all structures of FB, Bb and its homolog C2a, except for one covalently inhibited Bb structure<sup>24,26,28</sup> (**Supplementary Fig. 10d**). In the present low-resolution structure, no conformational changes were apparent in the SP domains of FB, Bb and C3bBb that would affect the catalytic site (**Supplementary Fig. 10e**), which would indicate that binding of C3b does not allosterically induce the catalytic activity of the protease fragment Bb.

C3b is probably critical in binding of the substrate C3 to the C3 convertase C3bBb; such an 'exosite' would explain the greater activity for the natural substrate C3 relative to that of five–amino acid peptides (with Michaelis constants of 6  $\mu$ M (ref. 27) and 210–3,000  $\mu$ M (ref. 29), respectively; plasma concentration of C3,  $\sim$ 5  $\mu$ M). We noted

a dimeric convertase complex that consisted of two opposing convertases created by the formation of C3b homodimers (**Fig. 2a**). The C3b dimer-formation face coincided with binding sites for the inhibitors compstatin<sup>30</sup>, CRIG<sup>16</sup> and antibody S77 (ref. 31), which block the binding of substrate to the C3 convertase. In the dimeric crystal structure, the C3b–C3b interface was formed by the MG4–MG5 domains of the C3b molecules (with buried surface areas of  $\sim$ 1,900–2,800  $\text{\AA}^2$ ; **Fig. 5a**). We generated a hypothetical enzyme–substrate (C3bBb–C3) complex by superposing the substrate C3 onto C3b based on the MG4–MG5 domains, with the observation that the arrangements of the MG1–MG6 domains (which form the  $\beta$ -ring) are strongly conserved between C3 and C3b (**Fig. 5b** and **Supplementary Fig. 11a** online). In the resulting C3bBb–C3 model, the catalytic site of C3bBb was oriented toward but positioned 30  $\text{\AA}$  away from the scissile loop of the substrate C3 (**Fig. 5b**). Furthermore, the homologous convertase C4b2a is expected to bind substrate C3 through the corresponding side of C4b, resulting in a similar C4b–C3 interface. The sequence alignment of the MG4–MG5 domains of C3, C4 and C5 indicated that many amino acid residues at the interaction site were

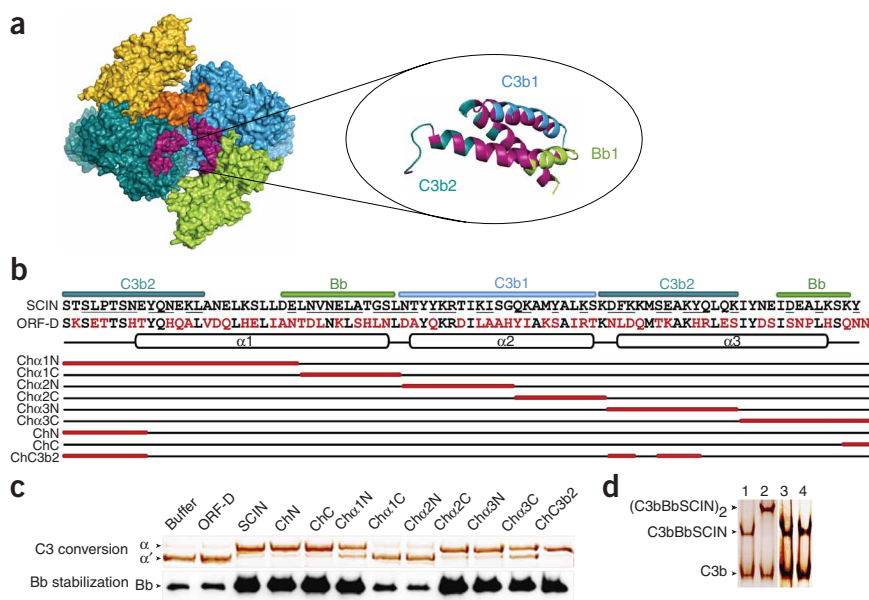


**Figure 3** Inhibition of C3bBb by SCIN.

(a) Contact sites of SCIN in the dimeric convertase, with the SCIN binding pocket presented in surface representation (left) and a ribbon diagram of SCIN with colors indicating molecular contacts (right). (b) Amino acid sequence alignment of SCIN and the nonfunctional homolog ORF-D. Convertase contact sites in SCIN are underlined. Below, SCIN chimeras (red boxes indicate exchanged segments). (c) Convertase inhibition by SCIN chimeras, with C3 conversion by fluid-phase C3bBb (above) and Bb stabilization on bacterial surfaces (below). (d) Native gel electrophoresis of convertases in the presence of Ni<sup>2+</sup> (lane 1), SCIN (lane 2), ChN (lane 3) or ChC3b2 (lane 4). Data (c,d) are representative of three independent experiments.

probably represents the product-release state C3bBb-C3b. Substrate binding putatively involves a larger area of C3 that includes the domains MG3 and MG6–MG8 at the same side as MG4–MG5 and hence closes part of

the gap between the substrate and the enzymatic complex. The differences in domain orientations of MG3, MG7 and MG8 (15°, 36° and 61°, respectively) in C3 (ref. 32) versus C3b<sup>15,16</sup> yield distinct shape complementarities and electrostatic surface potentials that could differentiate substrate binding from product release (Supplementary Fig. 12 online). SCIN possibly blocks both processes; it prevents swinging of Bb, and it may block a tighter C3b-C3 interface. In conclusion, the data suggest that the specific proteolytic activity of the C3bBb complexes is determined by the highly specific binding of the substrate through the ‘exosite’ located on the ligand C3b.

#### Intrinsic control of convertase activity

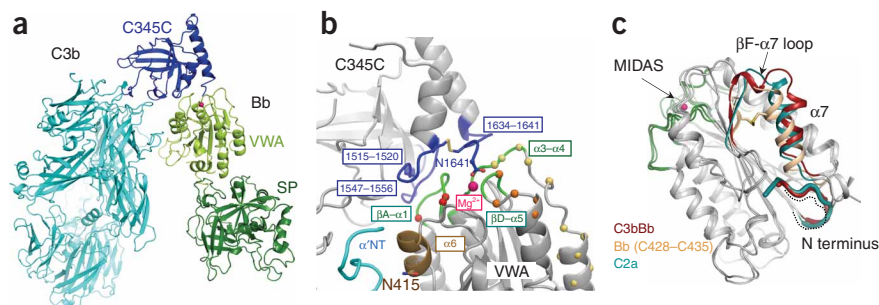
The C3 convertase (C3bBb) dissociates irreversibly, which is critical in controlling complement activation<sup>35</sup>. However, it is unclear what prevents the reassociation of Bb and C3b. Structural comparison of C3bBb with free Bb<sup>24</sup> and C3b<sup>15,16</sup> suggested that dissociation does not induce large conformational changes. Both free Bb<sup>24</sup> (as well as the isolated VWA domain<sup>36</sup>) and probably bound Bb have a MIDAS configuration that corresponds to the open, high-affinity state found in activated, ligand-binding integrin I $\alpha$  domains<sup>27</sup>. The possibility of putative changes in the helix  $\alpha$ 7 and the N-terminal tail of the VWA domain of Bb from the bound state to the dissociated state<sup>5,24</sup> was not supported by the available structural data (Fig. 4c and Supplementary Fig. 10). Surface plasmon resonance data show that the

conserved between C3 and C4 (ref. 32; Supplementary Fig. 11b). C5, however, differed both in amino acid sequence and in the domain-domain orientation of MG4–MG5, which may explain the weak interaction of C5 with C3b and poor cleavage of C5 by the C3bBb complex<sup>33,34</sup> (Supplementary Fig. 11a). These data indicated that the extreme specificity of the C3 convertase is possibly obtained by the formation of quasi-homodimers of C3 with C3b of the alternative pathway convertase (C3bBb) and a similar association of C3 to the evolutionary related C4b of the classical and lectin pathways convertase (C4b2a).

Positioning Bb of the C3bBb complex in place relative to the substrate C3 in the C3bBb-C3 model yielded a putative docking of the scissile loop into the active site of the SP domain in a productive (N-to-C) orientation (Fig. 5c). The observed orientation of the SP domain was consistent with the predicted orientation based on the crystal structure of C2a<sup>26</sup>, with the extended surface loops (unique to the chymotrypsin-like SP domains of Bb and C2a) folding along the anaphylatoxin domain of C3. Two possible concurrent effects may overcome the 30-Å gap between the catalytic site and the scissile loop and result into an enzymatically active complex. First, the large positional variation of the C345C domain in various C3b structures (Supplementary Fig. 9) suggests that the flexibility in C345C orientation may be used to swing Bb into place for proteolysis. Second, the observed C3b-C3b interface in the inhibited complex

**Figure 4** The C3bBb structure derived from the C3bBb-SCIN complex. (a) C3bBb complex, presented as a ribbon diagram with C3b in light and dark blue, Bb in light and dark green and Mg<sup>2+</sup> as a pink sphere. (b) The C345C-VWA interface between C3b and Bb, with the contact regions in blue (for the C345C domain of C3b) or green (for the VWA domain of Bb) and the disulfide bond of Cys1515–Cys1639 in C345C domain in a stick diagram. The residues substituted in FB chimeras are spheres (red,  $\beta$ A- $\alpha$ 1 loop; beige,  $\alpha$ 3- $\alpha$ 4 loop and  $\alpha$ 4 helix; orange,  $\beta$ D- $\alpha$ 5 loop), based on reference 22.

(c) Overlay of VWA domains of Bb in complex with C3b, Bb(C428–C435) (Protein Data Bank accession code 1RRK)<sup>24</sup> and C2a (Protein Data Bank accession code 2I6Q)<sup>26</sup>, showing the position of helix  $\alpha$ 7 and the nascent N terminus. The MIDAS loops  $\beta$ A- $\alpha$ 1,  $\alpha$ 3- $\alpha$ 4 and  $\beta$ D- $\alpha$ 5 are green; the N terminus of Bb (Cys428–Cys435) is missing (dashed line).



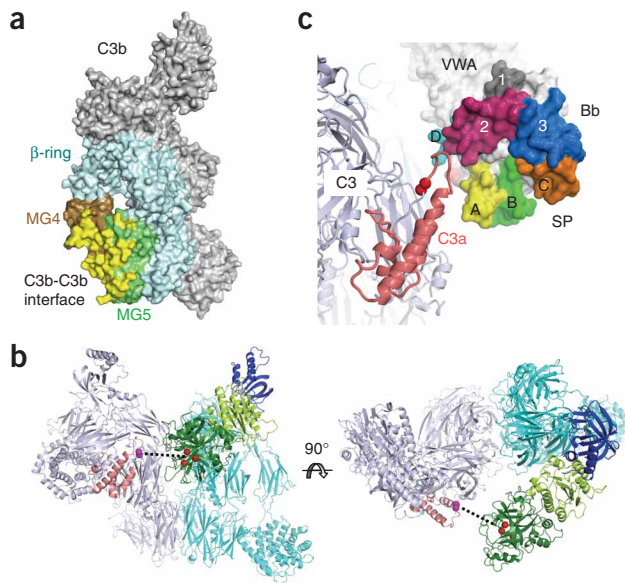


**Figure 5** The C3b-C3b interface and substrate-binding model. (a) Surface representation of C3b with the C3b-C3b dimer interface (yellow), which is formed by domains MG4 (brown) and MG5 (green) of the  $\beta$ -ring of C3b (MG1-MG6; cyan). (b) Model of the enzyme-substrate complex (C3bBb-C3), constructed by superimposition of C3 (Protein Data Bank accession code 2A73)<sup>32</sup> on the MG4-MG5 domains of the dimeric C3b molecule in the complex. Colors for C3bBb are as in **Figure 4a**; red spheres indicate the catalytic triad of Bb. The substrate C3 is gray, with the anaphylatoxin domain (C3a) highlighted in coral and the scissile bond (S726-R727) indicated by magenta spheres. The dashed line indicates the distance ( $\sim 30$  Å) between the catalytic site and the scissile loop. (c) Relative orientation of the C3a domain of C3 (substrate) and the surface loops of the SP domain of Bb forming the substrate-binding groove.

indicates that C3b of the enzyme complex (C3bBb) forms a dimer with its substrate C3 and provides an 'exosite' that determines the enzyme specificity.

On the basis of our results, we present a model for the activation of C3 by convertases. Surface-bound C3bBb binds the substrate C3 by forming a quasi-homodimer with C3b. Because Bb is bound to the flexible C345C domain in C3b, it can swing toward the substrate and cleave the scissile bond in C3. The C3a domain will be released, and conformational changes in C3b will induce its release from the enzyme complex. After diffusion, C3b may bind covalently to hydroxyl groups on the target surface through its reactive acyl-imidazole moiety<sup>4</sup>. Covalent binding to the surface without diffusion may generate C3b<sub>2</sub>Bb complexes with C5-convertase activity; this would explain the apparent discrepancy that formation of the C5 convertase depends on the binding of one C3b molecule<sup>8</sup> or multiple C3b molecules<sup>9</sup> to the C3 convertase complex. However, the precise arrangement of the multimolecular enzyme complex that leads to the binding and cleavage of C5 is unclear.

From an immune-evasion point of view, it is now understood that many amino acids in SCIN are involved in the formation of the dimeric inhibited convertase. In fluid phase, SCIN strongly binds to one convertase (C3bBb) and forms a bridge to the other convertase by binding C3b. By itself, the formation of convertase dimers could be an efficient convertase-inhibitory strategy, by preventing substrate binding. By altering the dimer-formation site in SCIN, we have shown that a monomeric SCIN-convertase is still an inhibited and stable complex. Thus, even if dimers cannot form on a bacterial surface, SCIN will block the C3bBb enzyme directly. Because we found a strong correlation between enzyme stability and inhibition by SCIN, we believe that SCIN prevents the swinging of Bb by fixing Bb on C3b. The dimeric nature of the convertase will contribute to complex stability and steric hindrance of the interactions of complement receptors with the stabilized convertase on the surface of the bacterium.

Although we can mimic these processes with purified components in solution, complement activation normally occurs on surfaces like those of bacteria. SCIN is a secreted bacterial molecule and has been shown to bind back to the surface as soon as active convertases are formed<sup>13</sup>. The secreted versus membrane-bound character of SCIN is critical in allowing this small molecule to fit in the narrow pocket of convertase components and to bind quickly to randomly distributed convertases at the bacterial surface. The similar activity of SCIN mutants on surface-bound and fluid-phase convertases suggests that the soluble complex is indeed representative of a surface-bound convertase. SCIN is an immunogenic bacterial protein and therefore is not suitable as an anti-inflammatory drug for humans. Nevertheless, the structure of the SCIN convertase provides insight into a unique and

proenzyme FB and C3b associate and dissociate in a two-step process in  $Mg^{2+}$ -containing buffer with one fast kinetic phase and one slow kinetic phase that differ by orders of magnitude<sup>37</sup>. Here, we extended that analysis by measuring the binding of FB to C3b in the absence of  $Mg^{2+}$  (to exclude the possibility of binding of the Bb fragment) and the interaction of fragment Ba with C3b (**Supplementary Fig. 13** online). Our data confirmed that Ba directly binds to C3b in a  $Mg^{2+}$ -independent way<sup>37,38</sup> and showed that binding of FB in the absence of  $Mg^{2+}$  shifted toward a kinetic profile similar to that of Ba. We therefore conclude that the fast on-off phase in the C3b-FB interaction is  $Mg^{2+}$  independent and can be attributed to initial contacts through the Ba segment. This result indicates that the Bb segment of FB associates and dissociates slowly. These data collectively indicate that the MIDAS and helix  $\alpha 7$  configuration in Bb establishes a stable ligand-binding site in the open configuration with slow association and dissociation kinetics, which is responsible for the intrinsic control of the convertase activity, the half-life and irreversible dissociation.

## DISCUSSION

Here we have shed important new light on the structure of the inherently unstable bimolecular C3 convertase (C3bBb), which is the central protease complex of the complement system, by demonstrating the dimeric structure of C3bBb stabilized by SCIN from *S. aureus*. The structure answered crucial questions related to convertase specificity and function relevant to understanding regulation of innate immunity. Furthermore, it showed in detail how bacteria may evade the immune system, which is important for understanding bacterial pathogenesis at the molecular level.

For the protection of host cells, complement activation is strictly regulated. Regulation occurs mainly at the level of C3 convertases, because the enzyme is a short-lived complex that cannot reassociate after dissociation. This first structure of C3bBb indicated that the conformation of Bb in the convertase complex is similar to that of Bb in its isolated form. Binding studies showed that Bb cannot rebind to C3b, because it has lost its fast association binding site for C3b, which is the Ba segment. Another critical aspect of complement regulation is that the C3 convertase enzyme is highly specific for C3 and does not or can hardly activate other proteins, such as the homologous C4 or C5. The presented structure of convertases in dimer formation

effective convertase-modulation strategy that evolved in a bacterial pathogen.

In summary, our data have provided insights into the molecular mechanisms that underlie the central amplification step of the complement system that leads to the opsonization of pathogens and altered host cells. These insights are essential for understanding the regulatory mechanisms of complement activation and the wide range of evasion strategies that can be used by pathogenic microorganisms. Both the structure and understanding of the convertase-inhibitory strategy provide crucial insights for the future development of complement inhibitors.

## METHODS

Methods and any associated references are available in the online version of the paper at <http://www.nature.com/natureimmunology/>.

**Accession code.** Protein Data Bank: coordinates and structure factors, 2WIN.

*Note: Supplementary information is available on the Nature Immunology website.*

## ACKNOWLEDGMENTS

We thank R. Romijn for help with mammalian protein expression; M. Otten and M. Daha for doing hemolytic assays; P. Lenting for help with Biacore analyses; the European Synchrotron Radiation Facility for synchrotron radiation facilities; and beamline scientists of the European Synchrotron Radiation Facility and the European Molecular Biology Laboratory for assistance. Supported by the Councils for Medical Sciences and Chemical Sciences of the Netherlands Organization for Scientific Research (S.H.M.R., J.A.G.v.S. and P.G.) and the US National Institutes of Health (J.D.L. and P.G.).

## AUTHOR CONTRIBUTIONS

J.W. expressed and purified FB and FD; M.R. and S.H.M.R. expressed and purified SCIN and chimeras; M.R. purified C3b; R.v.D., M.R. and S.H.M.R. generated and analyzed complexes and did functional assays; K.L.P. did and analyzed the analytical ultracentrifugation experiments; J.W. crystallized the complex and determined and analyzed the structure; B.J.C.J. helped with structure determination and analysis; A.T. expressed and purified Ba; D.R. did the C3b-FB and C3b-Ba binding studies; S.H.M.R., B.J.C.J., J.W., J.D.L., J.A.G.v.S. and P.G. conceived the experiments; and J.W., S.H.M.R., D.R., J.A.G.v.S. and P.G. wrote the manuscript.

Published online at <http://www.nature.com/natureimmunology/>

Reprints and permissions information is available online at <http://npg.nature.com/reprintsandpermissions/>

- Carroll, M.C. The complement system in regulation of adaptive immunity. *Nat. Immunol.* **5**, 981–986 (2004).
- Mollnes, T.E., Song, W.C. & Lambris, J.D. Complement in inflammatory tissue damage and disease. *Trends Immunol.* **23**, 61–64 (2002).
- Duncan, R.C., Wijeyewickrema, L.C. & Pike, R.N. The initiating proteases of the complement system: controlling the cleavage. *Biochimie* **90**, 387–395 (2008).
- Law, S.K. & Dodds, A.W. The internal thioester and the covalent binding properties of the complement proteins C3 and C4. *Protein Sci.* **6**, 263–274 (1997).
- Gros, P., Milder, F.J. & Janssen, B.J. Complement driven by conformational changes. *Nat. Rev. Immunol.* **8**, 48–58 (2008).
- Kerr, M.A. The human complement system: assembly of the classical pathway C3 convertase. *Biochem. J.* **189**, 173–181 (1980).
- Rawal, N. & Pangburn, M.K. C5 convertase of the alternative pathway of complement. Kinetic analysis of the free and surface-bound forms of the enzyme. *J. Biol. Chem.* **273**, 16828–16835 (1998).
- Kinoshita, T. *et al.* C5 convertase of the alternative complement pathway: covalent linkage between two C3b molecules within the trimolecular complex enzyme. *J. Immunol.* **141**, 3895–3901 (1988).
- Rawal, N. & Pangburn, M.K. Structure/function of C5 convertases of complement. *Int. Immunopharmacol.* **1**, 415–422 (2001).

- Kirkitadze, M.D. & Barlow, P.N. Structure and flexibility of the multiple domain proteins that regulate complement activation. *Immunol. Rev.* **180**, 146–161 (2001).
- Pangburn, M.K. & Muller-Eberhard, H.J. The C3 convertase of the alternative pathway of human complement. Enzymic properties of the bimolecular proteinase. *Biochem. J.* **235**, 723–730 (1986).
- Lambris, J.D., Ricklin, D. & Geisbrecht, B.V. Complement evasion by human pathogens. *Nat. Rev. Microbiol.* **6**, 132–142 (2008).
- Rooijackers, S.H. *et al.* Immune evasion by a staphylococcal complement inhibitor that acts on C3 convertases. *Nat. Immunol.* **6**, 920–927 (2005).
- Rooijackers, S.H. *et al.* Staphylococcal complement inhibitor: structure and active sites. *J. Immunol.* **179**, 2989–2998 (2007).
- Janssen, B.J., Christodoulidou, A., McCarthy, A., Lambris, J.D. & Gros, P. Structure of C3b reveals conformational changes that underlie complement activity. *Nature* **444**, 213–216 (2006).
- Wiesmann, C. *et al.* Structure of C3b in complex with CR1g gives insights into regulation of complement activation. *Nature* **444**, 217–220 (2006).
- Torreira, E., Tortajada, A., Montes, T., de Cordoba, S.R. & Llorca, O. 3D structure of the C3bB complex provides insights into the activation and regulation of the complement alternative pathway convertase. *Proc. Natl. Acad. Sci. USA* **106**, 882–887 (2009).
- Muller-Eberhard, H.J. & Gotze, O. C3 proactivator convertase and its mode of action. *J. Exp. Med.* **135**, 1003–1008 (1972).
- Fishelson, Z., Pangburn, M.K. & Muller-Eberhard, H.J. C3 convertase of the alternative complement pathway. Demonstration of an active, stable C3 C3b, Bb (Ni) complex. *J. Biol. Chem.* **258**, 7411–7415 (1983).
- Horiuchi, T., Macon, K.J., Engler, J.A. & Volanakis, J.E. Site-directed mutagenesis of the region around Cys-241 of complement component C2. Evidence for a C4b binding site. *J. Immunol.* **147**, 584–589 (1991).
- Hourcade, D.E., Mitchell, L.M. & Oglesby, T.J. Mutations of the type A domain of complement factor B that promote high-affinity C3b-binding. *J. Immunol.* **162**, 2906–2911 (1999).
- Tuckwell, D.S., Xu, Y., Newham, P., Humphries, M.J. & Volanakis, J.E. Surface loops adjacent to the cation-binding site of the complement factor B von Willebrand factor type A module determine C3b binding specificity. *Biochemistry* **36**, 6605–6613 (1997).
- Hourcade, D.E., Mitchell, L., Kuttner-Kondo, L.A., Atkinson, J.P. & Medof, M.E. Decay-accelerating factor (DAF), complement receptor 1 (CR1), and factor H dissociate the complement AP C3 convertase (C3bBb) via sites on the type A domain of Bb. *J. Biol. Chem.* **277**, 1107–1112 (2002).
- Ponnuraj, K. *et al.* Structural analysis of engineered Bb fragment of complement factor B: insights into the activation mechanism of the alternative pathway C3-convertase. *Mol. Cell* **14**, 17–28 (2004).
- Milder, F.J. *et al.* Factor B structure provides insights into activation of the central protease of the complement system. *Nat. Struct. Mol. Biol.* **14**, 224–228 (2007).
- Milder, F.J. *et al.* Structure of complement component C2a: implications for convertase formation and substrate binding. *Structure* **14**, 1587–1597 (2006).
- Luo, B.H., Carman, C.V. & Springer, T.A. Structural basis of integrin regulation and signaling. *Annu. Rev. Immunol.* **25**, 619–647 (2007).
- Krishnan, V., Xu, Y., Macon, K., Volanakis, J.E. & Narayana, S.V. The crystal structure of C2a, the catalytic fragment of classical pathway C3 and C5 convertase of human complement. *J. Mol. Biol.* **367**, 224–233 (2007).
- Kam, C.M. *et al.* Human complement proteins D, C2, and B. Active site mapping with peptide thioester substrates. *J. Biol. Chem.* **262**, 3444–3451 (1987).
- Janssen, B.J., Halff, E.F., Lambris, J.D. & Gros, P. Structure of compstatin in complex with complement component C3c reveals a new mechanism of complement inhibition. *J. Biol. Chem.* **282**, 29241–29247 (2007).
- Katschke, K.J. Jr. *et al.* Structural and functional analysis of a C3b-specific antibody that selectively inhibits the alternative pathway of complement. *J. Biol. Chem.* **284**, 10473–10479 (2009).
- Janssen, B.J. *et al.* Structures of complement component C3 provide insights into the function and evolution of immunity. *Nature* **437**, 505–511 (2005).
- Fredslund, F. *et al.* Structure of and influence of a tick complement inhibitor on human complement component 5. *Nat. Immunol.* **9**, 753–760 (2008).
- Rawal, N. & Pangburn, M. Formation of high-affinity C5 convertases of the alternative pathway of complement. *J. Immunol.* **166**, 2635–2642 (2001).
- Hourcade, D.E., Mitchell, L.M. & Medof, M.E. Decay acceleration of the complement alternative pathway C3 convertase. *Immunopharmacology* **42**, 167–173 (1999).
- Bhattacharya, A.A., Lupher, M.L., Jr., Staunton, D.E. & Liddington, R.C. Crystal structure of the A domain from complement factor B reveals an integrin-like open conformation. *Structure* **12**, 371–378 (2004).
- Harris, C.L., Abbott, R.J., Smith, R.A., Morgan, B.P. & Lea, S.M. Molecular dissection of interactions between components of the alternative pathway of complement and decay accelerating factor (CD55). *J. Biol. Chem.* **280**, 2569–2578 (2005).
- Prydzial, E.L. & Isenman, D.E. Alternative complement pathway activation fragment Ba binds to C3b. Evidence that formation of the factor B-C3b complex involves two discrete points of contact. *J. Biol. Chem.* **262**, 1519–1525 (1987).

## ONLINE METHODS

**Protein expression and purification.** C3 was purified from freshly isolated human plasma and C3b was generated as described<sup>39</sup>. After informed consent was provided by the donor, plasma was obtained at the University Medical Center Utrecht according to a study protocol approved by the medical ethics committee of the University Medical Center Utrecht. The preparation of recombinant SCIN and chimeric mutants has been described<sup>14</sup>. SCIN protein with an N-terminal six-histidine tag was prepared by overlap-extension PCR. In the ChC3b2 mutant, residues 1–13, 59–61, 64–65 and 67–68 were exchanged with corresponding residues of ORF-D. Plasma-purified FB and commercially obtained FD (Calbiochem) were used for Biacore, gel-filtration and small-scale experiments. For large-scale experiments in crystallization trials, recombinant FB and FD were used. Human FB fused to a N-terminal histidine tag containing a tobacco-etch virus protease cleavage site was expressed in human embryonic kidney 293S GnTI<sup>-</sup> (HEK293ES) cells to allow homogeneous N-linked glycosylation<sup>40</sup>. FB was purified by metal-affinity chromatography as described<sup>25</sup> and the histidine tag was removed by TEV protease cleavage and a second column passage on Ni-NTA Superflow beads (Qiagen). Finally, FB was purified by size-exclusion chromatography. Human FD was expressed without a tag in HEK293-EBNA cells (HEK293 cells that express Epstein-Bar virus nuclear antigen). Secreted FD was purified by cation-exchange and size-exclusion chromatography. Ba with a six-histidine tag at the N terminus was recombinantly expressed in a pQE30-M15 *Escherichia coli* expression system (Qiagen) and was purified from the inclusion bodies with a Ni-NTA Superflow column. After refolding, it was subjected to anion-exchange chromatography on a MonoQ1010 column.

**Binding convertase to immobilized SCIN.** CM5 sensor chips were immobilized with SCIN (2,526 resonance units) or CHIPS (3,372 resonance units; negative control)<sup>41</sup> by standard amine-coupling chemistry in 10 mM sodium acetate, pH 5. Purified C3b, FB and FD were passed over the surface at a flow rate of 30  $\mu$ l/min in HEPES-buffered saline (HBS)-Mg (20 mM HEPES, 140 mM NaCl, 5 mM MgCl<sub>2</sub> and 0.05% (vol/vol) Tween, pH 7.4); association and dissociation were both monitored for 300 s. Surfaces were regenerated with 0.1 M citric acid, 1 M NaCl and 1 mM EDTA, pH 5. Immobilization and binding experiments were done at 25 °C with a Biacore 2000.

**Gel filtration and native gel electrophoresis.** C3b (2  $\mu$ M), FB (2  $\mu$ M) and FD (1  $\mu$ M, Calbiochem) were incubated for 1 h at 4 °C in the presence of SCIN (4  $\mu$ M) or NiCl<sub>2</sub> (2.5 mM) in HBS-Mg and were separated on a Superdex-200 GL 10-mm  $\times$  300-mm column equilibrated with ice-cold HBS-Mg. The column was calibrated with the HMW Calibration kit (GE Healthcare) containing thyroglobulin (669 kDa), ferritin (440 kDa), aldolase (158 kDa), conalbumin (75 kDa) and ovalbumin (43 kDa). Alternatively, complexes were separated by native gel electrophoresis (7.5%) at 4 °C and were visualized by silver staining. C3 and FB were detected by immunoblot analysis<sup>13</sup>. SCIN was detected by enzyme-linked immunosorbent assay with mouse antibody to SCIN (anti-SCIN; 1C9) as a capturing antibody and biotinylated mouse anti-SCIN (2F4) for detection (both prepared 'in house')<sup>13</sup>; binding was visualized with peroxidase-conjugated streptavidin and tetramethyl benzidine substrate.

**Purification of SCIN-inhibited convertases for crystallization.** C3b (0.5  $\mu$ M), recombinant FB (1  $\mu$ M), recombinant FD (0.5  $\mu$ M) and histidine-tagged SCIN (2  $\mu$ M) were incubated for 1 h at 4 °C in 20 ml HBS-Mg. SCIN complexes were purified by incubation for 1 h at 4 °C with 1.2 g magnetic cobalt beads (Dynabeads Talon; Invitrogen). Beads were washed with HBS-Mg and complexes were eluted with 500 mM imidazole in 10 mM Tris, 40 mM NaCl and 5 mM MgCl<sub>2</sub>, pH 8 (2 ml). For removal of SCIN not in complex, complexes were washed with 200 ml buffer in a 100-kDa filter centricon device (Millipore); in a final centrifugation step, complexes were concentrated to  $\sim$ 5 mg/ml of purified complexes.

**Analytical ultracentrifugation.** A purified sample of the 500-kDa complex consisting of C3b, Bb and SCIN in 10 mM Tris, pH 8.0, 40 mM NaCl and 0.05% (vol/vol) Tween was used for a sedimentation-velocity experiment in an Optima XL-A analytical ultracentrifuge (Beckman Coulter). The sample, contained in a standard 12-mm Epon charcoal-filled centerpiece with quartz

windows, was diluted to obtain an absorbance of  $\sim$ 0.9 against a 'demi-water' reference, through a 12-mm path length at 229 nm for optimization of the signal/noise ratio. The sedimentation velocity run was done at 116,400g (An-50 Ti rotor) and 9.0 °C  $\pm$  0.3 °C during 2.5 h in which 140 scans were recorded at a radial step size of 30  $\mu$ m (data available at the UltraScan Van 't Hoff Laboratory Information Management System database as ExpDataID 74). A relative low angular velocity was chosen to retain sufficient shape information based on diffusion. Sedimentation velocity data were analyzed by enhanced van Holde-Weischet analysis<sup>42</sup> (UltraScan<sup>43</sup>) after subtraction of the time-invariant noise, which was determined in a two-dimensional spectrum analysis<sup>44</sup> (UltraScan). Sedimentation coefficients predicted from theory were calculated for the subunits with the assumption that they were spherical, prolate ellipsoidal and oblate ellipsoidal, and with buffer density and viscosity, as well as partial specific volumes calculated from the amino acid sequences (UltraScan<sup>43</sup>), accounted for (Supplementary Fig. 4d). For the last two shapes, an arbitrary axial or aspect ratio of 6 was taken. On the basis of sedimentation-velocity simulations (UltraScan), the dimeric complex (C3bBb-SCIN)<sub>2</sub> has a predicted sedimentation coefficient between 10 S and 20 S (1 S  $\equiv$  1  $\times$  10<sup>-13</sup> s).

**Crystallization, data collection and structure determination.** Freshly purified SCIN-stabilized complexes were set up for crystallization trials by hanging-drop vapor diffusion at 4 °C. Crystals appeared overnight and grew within 2 weeks to a typical size of 300  $\times$  100  $\times$  40  $\mu$ m<sup>3</sup> in many conditions. Over 100 crystals were screened at European Synchrotron Radiation Facility beamline (ID14-EH14). Most crystals diffracted between 4 Å and 5 Å; only one crystal diffracted at a resolution of better than 4 Å. A complete data set was collected from this crystal, which diffracted to a resolution of 3.9 Å. This crystal was grown in the condition of 75 mM sodium-potassium tartrate, 8.0% (wt/vol) PEG 3350 and 50 mM Bis-Tris propane, pH 6.5. The crystal was in space group P2<sub>1</sub> ( $a$  = 228.6 Å,  $b$  = 121.5 Å,  $c$  = 280.8 Å,  $\alpha$  = 90°,  $\beta$  = 91.6°, and  $\gamma$  = 90°). The data set was integrated and scaled with the programs MOSFLM and Scala<sup>45</sup>. The asymmetric unit contained four C3bBb-SCIN complexes arranged as two dimers. The structure was solved by molecular replacement with the PHASER program<sup>46</sup> with the isolated structures of C3c (2A74)<sup>32</sup>, C3b (2I07)<sup>15</sup>, Bb (1RRK)<sup>24</sup> and SCIN (2QFF)<sup>14</sup> as the initial search models (Protein Data Bank accession codes in parentheses). The automatic searches for the CUB, TED and C345C domains of C3b and SCIN in PHASER yielded only two copies of each domain or protein. The missing parts were placed manually by superposition and were adjusted by rigid-body refinement in PHASER to obtain a complete model. One C3b molecule lacked density for its TED because of disorder; occupancies were set to 0.0 for this domain. The C3b molecule in this copy (copy 4) had a weaker density than C3b in other copies (Supplementary Fig. 6). The model was rebuilt with the Crystallographic Object-Oriented Toolkit system<sup>47</sup>, and refinement was done with PHENIX software<sup>48</sup>. Tight fourfold noncrystallographic symmetry restraints were used for the following domains or molecules: MG1, MG2, MG3, MG4, MG5, MG6, linker,  $\alpha'$  N-terminal tail and MG7, MG8, CUB of C3b; VWA and SP of Bb and SCIN. Tight threefold noncrystallographic symmetry restraints were used for TEDs in copies of 1–3. Twofold noncrystallographic symmetry restraints were used for C345C domains (copies of 1 and 3 as a group and copies of 2 and 4 as a group). The final  $R_{\text{work}}$  and  $R_{\text{free}}$  values were 25.3% and 26.8%, respectively.

**Convertase inhibition assays.** C3 (250 nM), C3b (50 nM), FB (500 nM), FD (500 nM) and SCIN chimeras (2  $\mu$ M) were incubated for 10 min at 20 °C in HBS-Mg, and C3 conversion was analyzed by SDS-PAGE in reducing conditions. Convertase stabilization on bacteria was done as described<sup>14</sup>. HBS-Mg-EGTA instead of HBS-Mg<sup>2+</sup>-Ca<sup>2+</sup> was used for induction of only the alternative pathway.

**Kinetic analysis of FB and Ba interaction with C3b.** Kinetics were profiled by surface plasmon resonance (Biacore 2000) at 25 °C. C3b was biotinylated at its thioester moiety and captured on a streptavidin-coated sensor chip. FB (63 nM–2  $\mu$ M) was injected for 3 min at a flow rate of 30  $\mu$ l/min and dissociation was monitored for 5 min. The surface was regenerated with 2 M NaCl and 0.2 M sodium carbonate, pH 9.0, for 30 s each. Fragment Ba (40 nM–40  $\mu$ M) was injected for 1 min at a flow rate of 30  $\mu$ l/min with a dissociation phase of 2 min and a short regeneration pulse (20 s) of 1 M NaCl. All binding

experiments were repeated in running buffer (10 mM HEPES, pH 7.4, 150 mM NaCl and 0.005% (vol/vol) Tween-20) containing either 1 mM MgCl<sub>2</sub> or 3 mM EDTA. Signals from an untreated streptavidin surface and an ensemble of buffer blank injections were subtracted from the binding signals. Data were processed with Scrubber (BioLogic Software), and CLAMP software<sup>49</sup> was used for kinetic analysis.

39. Lambris, J.D., Dobson, N.J. & Ross, G.D. Release of endogenous C3b inactivator from lymphocytes in response to triggering membrane receptors for  $\beta$ 1H globulin. *J. Exp. Med.* **152**, 1625–1644 (1980).
40. Reeves, P.J., Callewaert, N., Contreras, R. & Khorana, H.G. Structure and function in rhodopsin: high-level expression of rhodopsin with restricted and homogeneous N-glycosylation by a tetracycline-inducible N-acetylglucosaminyltransferase I-negative HEK293S stable mammalian cell line. *Proc. Natl. Acad. Sci. USA* **99**, 13419–13424 (2002).
41. de Haas, C.J. *et al.* Chemotaxis inhibitory protein of *Staphylococcus aureus*, a bacterial antiinflammatory agent. *J. Exp. Med.* **199**, 687–695 (2004).

42. Demeler, B. & van Holde, K.E. Sedimentation velocity analysis of highly heterogeneous systems. *Anal. Biochem.* **335**, 279–288 (2004).
43. Demeler, B. in *Analytical Ultracentrifugation: Techniques and Methods* (eds. Scott, D.J., Harding S.E. & Rowe, A.J.) 210–230 (Royal Society of Chemistry, Cambridge, 2005).
44. Brookes, E. & Demeler, B. Parallel computational techniques for the analysis of sedimentation velocity experiments in UltraScan. *Colloid Polym. Sci.* **286**, 139–148 (2008).
45. Evans, P. Scaling and assessment of data quality. *Acta Crystallographica Section D* **62**, 72–82 (2006).
46. McCoy, A.J. *et al.* Phaser crystallographic software. *J. Appl. Cryst.* **40**, 658–674 (2007).
47. Emsley, P. & Cowtan, K. Coot: model-building tools for molecular graphics. *Acta Crystallogr. D Biol. Crystallogr.* **60**, 2126–2132 (2004).
48. Adams, P.D. *et al.* PHENIX: building new software for automated crystallographic structure determination. *Acta Crystallogr. D Biol. Crystallogr.* **58**, 1948–1954 (2002).
49. Myszka, D.G. & Morton, T.A. CLAMP: a biosensor kinetic data analysis program. *Trends Biochem. Sci.* **23**, 149–150 (1998).